Relativistic-configuration-interaction calculations of $K\alpha$ satellite properties for aluminum plasmas created by intense proton beams

Ping Wang, Joseph J. MacFarlane, and Gregory A. Moses
Fusion Technology Institute, Department of Nuclear Engineering and Engineering Physics, University of Wisconsin–Madison, Madison, Wisconsin 53706
(Received 1 October 1992; revised manuscript received 14 June 1993)

Configuration-interaction calculations with Breit-Pauli relativistic corrections have been carried out for aluminum ions for the purpose of studying $K\alpha$ satellite spectra obtained during intense proton-beam–plasma interaction experiments. We present results for calculated wavelengths, oscillator strengths, and fluorescence yields of $K\alpha$ satellites for Al I–Al XI. Detailed calculations have been performed both for transitions involving levels of ground-state configurations and for transitions involving levels of low-lying excited configurations with M-shell spectator electrons. Calculated wavelengths for the $K\alpha$ transitions are compared with a spectrum obtained during a Particle Beam Fusion Accelerator II proton-beam experiment [Lasers Part. Beams **8**, 555 (1990)] at Sandia National Laboratories. Our calculations show that the $K\alpha$ satellite lines of aluminum ions can be classified into two distinct groups: one involving transitions of type $1s^1 2s^r 2p^q \rightarrow 1s^2 2s^r 2p^{q-1}$, the other $1s^1 2s^r 2p^{q-1} 3l \rightarrow 1s^2 2s^r 2p^{q-2} 3l$. The former consists of the resonance $K\alpha$ transitions, which gives the characteristic satellite-line position of an ion, while the latter overlaps with the resonance $K\alpha$ lines of the next-higher ionization stage. We find that both correlation effects and relativistic corrections significantly impact the calculated $K\alpha$ transition energies.

PACS number(s): 52.25.Nr, 32.30.Rj, 32.70.−n, 32.80.Hd

I. INTRODUCTION

Atomic inner-shell x-ray spectroscopy has been widely used to diagnose plasma conditions in targets irradiated by intense laser or ion beams [1–6]. For low- and medium-Z elements (atomic number $Z \leq 30$), the absorption and emission spectroscopy of K-shell lines can be particularly useful. $K\alpha$ emission lines result from transitions between an atomic state having at least one vacancy in the $1s$ shell and a state in which an electron from the $2p$ subshell fills this vacancy. The $K\alpha$ emission lines corresponding to transitions from initial states having one hole in the K shell and n holes in the L shell are the satellite $K\alpha$ lines. These satellite $K\alpha$ lines are blue shifted with respect to the principal $K\alpha$ lines because of the reduced screening of the nucleus which results when there are fewer spectator electrons in the L shell. In the case of low- and medium-Z elements, the energy shift (the distance between the consecutive satellites) caused by introducing an additional hole in the L shell ($\lambda/\Delta\lambda \geq 10^2$) is readily observable in present-day laboratory plasma experiments. For present-day light-ion beam-heated plasmas ion beam-impact ionization produces K-shell vacancies which lead to the formation of $K\alpha$ emission satellite spectra. Hence, there is a one-to-one correspondence between resonance $K\alpha$ satellite lines and ionization states. It has been suggested that this characteristic of $K\alpha$ emission satellite spectra can be used as a temperature diagnostic for plasmas heated by light-ion beams in inertial-fusion experiments [5,6]. Light-ion impact ionization of K-shell electrons populates autoionizing states, which then produce fluorescence $K\alpha$-line emission. Since the $K\alpha$ satellite lines from Ne-like to He-like ions exhibit detectable shifts to shorter wavelengths, $K\alpha$ emission satellite spectra can provide a measure of the ionization distribution in a plasma and, from that, constraints on plasma conditions.

The first spectroscopic observation of $K\alpha$ x-ray satellite lines in an intense-proton-beam experiment was recently made during a Particle Beam Fusion Accelerator II (PBFA-II) experiment at Sandia National Laboratories [6]. In this experiment an aluminum target was irradiated with a 4–6-MeV, 1–2-TW/cm^2 proton beam. An elliptic crystal spectrograph with a resolution of $\lambda/\Delta\lambda \geq 1200$ was used to obtain a time-integrated spectrum. The experimental $K\alpha$ satellite spectrum was observed to have two important features. First, there is a high degree of structure in the spectrum which is likely caused by term-dependent $K\alpha$ transitions. It is important to be able to identify these structures for the purpose of diagnosing plasma conditions. In addition, the satellite line shapes are very broad. It has been found [7,8] that this broad line shape comes from the contributions of the $K\alpha$ satellite lines that are produced by transitions of the general type

$$1s^2 2s^r 2p^q nl \rightarrow 1s^2 2s^r 2p^{q-1} nl \ ,$$

primarily with $n=3$. For the electron temperature and density conditions in present-day light-ion beam-heated plasmas ($T_e < 10^2$ eV and $N_e \sim 10^{20}$ cm^{-3}), the Stark broadening effects can be very significant for these satellite lines. This suggests that it is necessary to consider the satellite lines from excited configurations with M-shell spectator electrons in analyzing the experimental $K\alpha$ spectrum.

With spectral resolutions of $\lambda/\Delta\lambda \sim 1500$ in the present experiments, it is preferable to determine transition energies to the accuracy of a few parts in 10^4 to reduce uncertainties in line identification. To accurately compute wavelengths for transitions between the K and L shells of medium-Z ions, both relativistic and correlation effects must be included in determining the transition energies. Several theoretical calculations on the $K\alpha$ x-ray spectra of medium-Z elements have been performed to study the $K\alpha$ satellite structures [3,9,10]. These calculations, however, neglect either relativistic corrections or correlation effects. There are typical uncertainties of 0.1% to 0.3% in the wavelengths of these calculations. Furthermore, no systematic calculations have been done for aluminum $K\alpha$ satellite structure with the inclusion of transitions of the type

$$1s^2 2s^r 2p^q nl \rightarrow 1s^2 2s^r 2p^{q-1} nl$$

with $n \geq 3$.

In this investigation, calculation results are presented for the $K\alpha$ satellite emission lines produced by the $2p \rightarrow 1s$ inner-shell electron radiative transitions in the aluminum ions from Al I to Al XI (here and through the rest of this paper, the designation for ions is for the ionization stage before the K-shell ionization by ion impact). These radiative transitions give rise to prominent satellite lines in the x-ray region from 7.75 to 8.35 Å. Configuration-interaction calculations with Breit-Pauli relativistic corrections have been carried out for the $K\alpha$ transitions of the types

$$1s^2 2s^r 2p^q \rightarrow 1s^2 2s^r 2p^{q-1}$$

and

$$1s^1 2s^r 2p^{q-1} nl \rightarrow 1s^2 2s^r 2p^{q-2} nl \ .$$

The purpose of the calculations is to provide accurate transition energies, oscillator strengths, and term-dependent fluorescence yields for analyzing aluminum $K\alpha$ spectra in light-ion fusion experiments. In our calculations, we first performed multiconfiguration Hartree-Fock (MCHF) calculations [11] to determine a basis for the representation of the states of interest. Then a configuration-interaction calculation within the Breit-Pauli approximation was performed. In this way, both relativistic and correlation effects can be accounted for properly.

II. CALCULATIONS

Our calculations for atomic energy levels and radiative transition probabilities were performed using our configuration-interaction (CI) code CIBASE, which is based on the modification of Fraga's configuration-interaction program RIAS [12]. Term-dependent fluorescence yields were calculated using our computer code ACKF with MCHF wave functions. A brief overview of the calculation method is given in this section.

The CI wave functions for each atomic state are represented by expansions of the form

$$\Psi(J,M_J) = \sum_{i=1}^{N} a_i \Phi(\alpha_i L_i S_i, JM_J) \ , \tag{1}$$

where N is in principle infinite, but for all practical calculations is finite; $\{\Phi_i\}$ is a set of "configuration wave functions," each describing a configuration, and is constructed from one-electron functions with $\{\alpha_i\}$ defining the coupling scheme of angular momenta of the electrons. The Hamiltonian matrix, with typical element $\langle \Phi_i | H | \Phi_j \rangle$, can be diagonalized to give eigenvalues $E_1 < E_2 < \cdots < E_N$. Then from the Hylleraas-Undheim-MacDonald theorem [13], we have

$$E_k \geq E_k^{\text{exact}} \ . \tag{2}$$

The wave function associated with a particular eigenvalue (eigenenergy E_k) is then given by Eq. (1) with the $\{a_i\}$ taken to be the corresponding eigenvector components:

$$\sum_{j=1}^{N} (H_{ij} - E_k \delta_{ij}) a_j = 0 \ , \quad j = 1,2,\ldots,N \ . \tag{3}$$

In the intermediate-coupling scheme, the sum over i in the expansion includes N configurations in which the orbital L_i and spin S_i angular momenta couple to give the total angular momentum

$$J = L_i + S_i \ . \tag{4}$$

Each one-electron function is the product of a radial function, a spherical harmonic, and a spin function. The configuration functions $\{\Phi_i\}$, and hence the eigenvalues $\{E_k\}$, depend on the choice of radial functions $\{P(nl|r)\}$. The inequalities of Eq. (2) allow any of the eigenvalues to be used as the functional to be minimized with respect to variations in the radial functions. In this study, the multiconfiguration Hartree-Fock calculations were performed using Froese Fischer's program MCHF77 [11] to obtain radial wave functions. The calculations were carried out for the lowest state of each principal configuration under consideration, and included configurations that involved all the orbitals to be used in the CI calculations. The radial functions obtained in such a way are ensured to be orthonormal automatically. It should be noted that we used the Breit-Pauli Hamiltonian only for determining the mixing coefficients a_i appearing in CI expansions and not for the optimization of the radial functions.

The Hamiltonian operator considered in this work may be written as

$$H = H_{\text{el}} + H_{\text{SM}} + H_{\text{rel}} \ , \tag{5}$$

where H_{el} denotes the electronic Hamiltonian (consisting of the electron kinetic, nuclear attraction, and electrostatic-repulsion energy terms), H_{SM} denotes the operator for the specific-mass effect, and

$$H_{\text{rel}} = H_{LS} + H_{fs} \tag{6}$$

includes the usual relativistic corrections: H_{LS} consists of the so-called L-S-non-splitting terms (mass variation, Darwin corrections, and electron spin-spin contract and orbit-orbit interactions), H_{fs} includes the fine-structure

TABLE I. Calculated wavelengths (Å) for the term-dependent transitions of Al V.

Transitions	HF	HF+BP	MCHF	CI+BP	Chenais-Popovics [3]
$1s^1 2s^2 2p^5 \rightarrow 1s^2 2s^2 2p^4$					
$^1P^o \rightarrow {}^1S$	8.293	8.281	8.295	8.287	
$^1P^o \rightarrow {}^1D$	8.261	8.248	8.264	8.258	8.249
$^3P^o \rightarrow {}^3P$	8.273	8.257	8.278	8.269	8.259
$1s^1 2s^2 2p^6 \rightarrow 1s^2 2s^1 2p^5$					
$^3S \rightarrow {}^3P^o$	8.270	8.265	8.272	8.267	8.264
$^1S \rightarrow {}^1P^o$	8.357	8.343	8.359	8.349	

(electron spin–own-orbit, spin–other-orbit, and spin-spin dipole) couplings. Detailed expressions for each of these operators have been given in the literature [14,15].

Once wave functions in the form of Eq. (1) have been determined, they are used to obtain oscillator strengths for transitions between initial and final states Ψ^i and Ψ^j with energies E^i and E^j:

$$g_i f(i \rightarrow j) = \frac{2\Delta E}{3} \left| \left\langle \Psi^i \left| \sum_p \mathbf{r}_p \right| \Psi^j \right\rangle \right|^2 , \tag{7}$$

where $\Delta E = |E^i - E^j|$, g_i is the degeneracy of initial state i with

$$g_i = (2L_i + 1)(2S_i + 1)$$

for L-S coupling, and $g_i = 2J_i + 1$ for intermediate coupling.

In the results presented in this paper, the intensity of the transition $i \rightarrow f$ is given by

$$I(i\text{-}f) = \omega_i \frac{\Gamma_R(i\text{-}f)}{\sum_j \Gamma_R(i\text{-}j)} , \tag{8}$$

where $I(i\text{-}f)$ is the stick intensity of transition $i \rightarrow f$ (i.e., frequency-integrated over the line), ω_i is the fluorescence yield for the autoionizing state i, and $\Gamma_R(i\text{-}j)$ is the radiative decay rate from state i to state j. Term-dependent fluorescence yields were calculated by the expression

$$\omega_i = \frac{\Gamma_R(i)}{\Gamma_A(i) + \Gamma_R(i)} . \tag{9}$$

Here the radiative decay rates $\Gamma_R(i)$ are deduced from the corresponding transition energies and oscillator strengths, while the Auger transition rates $\Gamma_A(i)$ are calculated using the L-S-coupling formalism of Asaad and Burhop [16] with MCHF wave functions.

III. RESULTS AND DISCUSSION

A. Effects of correlation and relativistic corrections on the $K\alpha$ transition energies

The salient feature of $K\alpha$ transitions is the inclusion of K- and L-shell electrons. It was therefore important to examine the effects of both correlation and relativistic corrections on the $K\alpha$ transition energies.

To study this problem, we have used four different approaches to calculate the transition energies for the term-dependent transitions of

$$1s^1 2s^2 2p^5 \rightarrow 1s^2 2s^2 2p^4$$

and

$$1s^1 2s^1 2p^6 \rightarrow 1s^2 2s^1 2p^5$$

in Al V: (1) nonrelativistic single-configuration Hartree-Fock (HF), (2) single-configuration Hartree-Fock with Breit-Pauli relativistic corrections (HF+BP), (3) nonrelativistic multiconfiguration Hartree-Fock (MCHF), and (4) configuration interaction with Breit-Pauli relativistic corrections (CI+BP). The calculated results are collected in Table I. Also given in Table I are the theoretical values of Chenais-Popovics *et al.* [3] which are calculated using a relativistic parametric potential method [17]. The corresponding configurations used in the CI expansions are listed in Table II.

Two things should be noted from the results in Table I. First, our HF+BP results are very close to those of Chenais-Popovics *et al.* This is because both calculations neglected the correlation effect while including relativistic corrections. Second, if we take the results of CI+BP as a reference, it is seen that the wavelengths obtained from the MCHF calculations have a redshift, while the wavelengths obtained from the HF+BP calculations have a blueshift. The results of the HF calculation are closer to the results of the CI+BP calculation than the others. In general, the relativistic effects are the strongest for inner-shell electrons, while the correlation effects are the strongest for outer atomic shells. Hence, it can be expected that the correlation corrections for the upper-state ($1s^1 2s^2 2p^5$ and $1s^1 2s^1 2p^6$) energies are stronger than those for the lower state ($1s^2 2s^2 2p^4$ and $1s^2 2s^1 2p^5$) energies, and vice versa for the relativistic corrections.

TABLE II. Configurations used in the CI expansions for Al V calculations.

$^1P^o, {}^3P^o$	^1S	$^1D, {}^3P$
$1s^1 2s^2 2p^5$	$1s^1 2s^2 2p^4$	$1s^2 2s^2 2p^4$
$1s^1 2p^5 3s^2$	$1s^2 2p^6$	$1s^2 2p^4 3s^2$
$1s^1 2s^2 2p^3 3s^2$	$1s^2 2p^4 3s^2$	$1s^2 2s^2 2p^2 3s^2$
$1s^1 2s^2 2p^3 3p^2$	$1s^2 2s^2 2p^2 3s^2$	$1s^2 2s^2 2p^2 3p^2$
$1s^1 2s^2 2p^3 3d^2$	$1s^2 2s^2 2p^2 3p^2$	$1s^2 2s^2 2p^2 3d^2$
$1s^1 2s^2 2p^4 3p^1$	$1s^2 2s^2 2p^2 3d^2$	$1s^2 2s^2 2p^3 3p^1$
$1s^1 2s^2 2p^4 4f^1$	$1s^2 2s^2 2p^3 3p^1$	$1s^2 2s^2 2p^3 4f^1$
$1s^1 2s^1 2p^5 3d^1$	$1s^2 2s^1 2p^4 3d^1$	$1s^2 2s^1 2p^4 3d^1$

This is why one sees a blueshift in the $K\alpha$ transition energies when the relativistic corrections are included, while a redshift occurs when the correlation effect is included. Since the relativistic and correlation effects cause opposing shifts in the $K\alpha$ transition energies, they cancel each other to some degree. Because of this, nonrelativistic single-configuration Hartree-Fock calculation can sometimes provide reasonably good results. However, it must be noted that relativistic and correlation effects do not cancel each other *exactly*. One can expect that relativistic effects will become more important for higher ionization stages. This suggests that to obtain accurate term-dependent $K\alpha$ transition energies, both relativistic and correlation effects must be accounted for properly.

Figure 1 shows a comparison of the calculated wavelengths of CI+BP for Al V $K\alpha$ satellites and the PBFA-II experimental data. The three features in the Al V satellites are attributed to the term-dependent transitions of

$$1s^1 2s^2 2p^5 \rightarrow 1s^2 2s^2 2p^4$$

and

$$1s^1 2s^1 2p^6 \rightarrow 1s^2 2s^1 2p^5 .$$

Very good agreement is achieved. The good agreement between the calculated wavelengths and the experimental data allows us to determine confidently the transitions that are responsible for peaks in the experimental spectrum.

B. Term-dependent $K\alpha$ Auger rates and fluorescence yields for aluminum ions

Accurate K-shell Auger rates and fluorescence yields are critical for the interpretation of observed $K\alpha$ emission satellite spectra. We have calculated term-dependent K-shell Auger rates and fluorescence yields for aluminum ions with electronic configurations of type $1s^1 2s^q 2p^r 3l^t$ ($q \geq 0$, $r \geq 1$, and $t \geq 0$). Some of our calculated results are listed in Table III and are compared with the theoretical results of Combet Farnoux [18]. It can be seen that the two sets of data are in good agreement. All related term-dependent fluorescence yields are presented in Fig. 2. Also given in the figure are the corresponding configuration-averaged fluorescence yields. As shown, for an ion with an inner-shell hole and a partially filled outer shell, the fluorescence yields of the autoionizing state can differ by orders of magnitude among various L-S terms of a given initial hole electronic configuration. This is a very important point in analyzing inner-shell x-ray emission spectra.

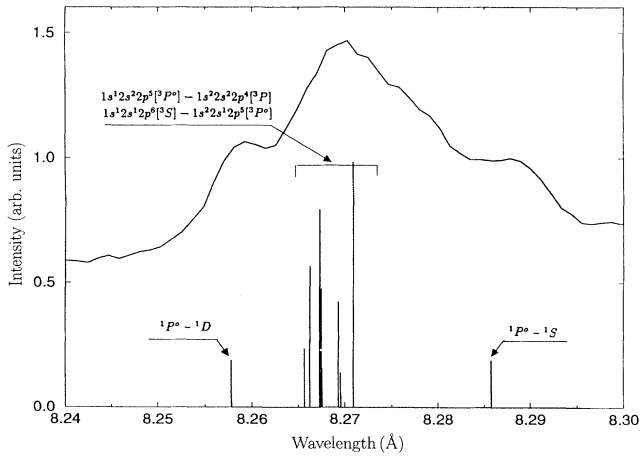

FIG. 1. Comparison of the calculated wavelengths and relative intensities with the PBFA-II experimental data. The stick spectrum represents the lines associated with the transitions $1s^1 2s^2 2p^5 \rightarrow 1s^2 2s^2 2p^4$ and $1s^1 2s^1 2p^6 \rightarrow 1s^2 2s^1 2p^5$.

C. Structure of the $K\alpha$ satellite lines for Al I through Al XI

$K\alpha$ radiation can occur only if an ion is momentarily raised to an excited configuration that has one or more $2p$ electrons and a $1s$ hole. In intense-proton-beam-heated plasmas, photoionization, photoexcitation, inner-shell electron collision excitation, and dielectronic recombination are unimportant for producing such an autoionizing configuration. The main mechanism by which a $1s$ hole can be produced is inner-shell ion impact ionization. If essentially all ions lie in the ground configuration, the structure of the $K\alpha$ satellite spectra would be relatively simple because beam-induced multiple-ionization effects are unimportant in a proton-beam-heated Al plasma. However, excitation and ionization by thermal electrons produce a distribution of populations in the bulk plasma. For aluminum ions at the plasma conditions of interest here, the populations of excited electronic configurations of type $1s^2 2s^2 2p^r 3l^1$ can be appreciable and can have significant contributions to the observed spectra [7,8]. In such cases, the structure of $K\alpha$ satellite spectra becomes very complicated because of the substantial contributions from ions in excited electronic configurations. We illustrate these using the special case of $K\alpha$ emissions from ions with five $2p$ electrons and a $1s$ hole as follows.

(a) Electron collisional ionization out of the $2p$ shell from $1s^2 2s^2 2p^6$:

$$1s^2 2s^2 2p^6 \xrightarrow[\text{thermal ionization}]{} 1s^2 2s^2 2p^5 . \tag{10}$$

(b) Electron collisional excitation out of the $2p$ shell from $1s^2 2s^2 2p^6$:

$$1s^2 2s^2 2p^6 \xrightarrow[\text{thermal excitation}]{} 1s^2 2s^2 2p^5 nl^1 . \tag{11}$$

(c) Proton impact ionization out of the $1s$ shell from $1s^2 2s^2 2p^5$ followed by a spontaneous fluorescence transition:

$$1s^2 2s^2 2p^5 \xrightarrow[\text{beam ionization}]{} 1s^1 2s^2 2p^5 \xrightarrow[K\alpha \text{ fluorescence decay}]{} 1s^2 2s^2 2p^4 . \tag{12}$$

(d) Proton impact ionization out of the $1s$ shell from $1s^2 2s^2 2p^5 nl^1$ followed by a spontaneous fluorescence transition:

TABLE III. Term-dependent Auger and radiative transition rates, and fluorescence yields for $1s^1 2s^2 sp^r$ of Al.

Configuration	LS	Auger rate[a]	Radiative rate[a]	$\omega_K(LS)$	$\omega_K(LS)$ (Combet Farnoux) [18]
$1s^1 2s^2 2p^6$	^2S	130.05	6.26	0.0459	0.0462
$1s^1 2s^2 2p^5$	^1P	103.99	8.95	0.0793	0.0814
	^3P	113.67	4.53	0.0383	0.0393
$1s^1 2s^2 2p^4$	^2S	89.50	4.88	0.0517	0.0543
	^2P	73.16	9.63	0.1164	0.1258
	^4P	88.71	2.46	0.0270	0.0290
	^2D	102.48	4.86	0.0453	0.0475
$1s^1 2s^2 2p^3$	^3S	31.53	10.37	0.2474	0.3152
	^5S	52.36	0.0	0.0	0.0
	^1P	59.80	7.77	0.1149	0.1283
	^3P	71.38	2.65	0.035 78	0.0397
	^1D	69.10	12.59	0.1541	0.1112
	^3D	81.21	2.63	0.0314	0.0347
$1s^1 2s^2 2p^2$	^2S	48.55	2.836	0.055 18	0.0654
	^2P	27.51	8.309	0.2320	0.308
	^4P	45.25	0.0	0.0	0.0
	^2D	64.48	2.815	0.041 84	0.0482

[a]In multiples of 10^{-4} a.u., 1 a.u. $=4.134\times10^{16}$ s^{-1}.

$$1s^2 2s^2 2p^5 nl^1 \xrightarrow[\text{beam ionization}]{} 1s^1 2s^2 2p^5 nl^1 \xrightarrow[K\alpha \text{ fluorescence decay}]{} 1s^2 2s^2 2p^4 nl^1 \ . \quad (13)$$

It should be noted that the thermal excitation process of

$$1s^2 2s^2 2p^6 nl^1 \xrightarrow[\text{thermal excitation}]{} 1s^2 2s^2 2p^5 nl^1 (n'l')^1 \quad (14)$$

is just as likely as the excitation process of (b). However, since doubly excited configurations are generally at high energies with respect to the ground state, their populations are very small and one would expect their contribution to the proton-beam-induced $K\alpha$ spectrum to be unobservable. The substantial contributions to the observed $K\alpha$ satellite spectra of a proton-beam-heated plasma are from ions with initial electronic configurations in the ground configuration and the low-lying excited configurations of type $1s^2 2s^r 2p^s nl^1$. The transition array of type

$$1s^1 2s^r 2p^s nl^1 \rightarrow 1s^2 2s^r 2p^{s-1} nl^1$$

involves numerous spectrum lines because the excited configuration possesses many energy levels. These lines cover the same wavelength range as lines of the transition array

$$1s^1 2s^r 2p^s \rightarrow 1s^2 2s^r 2p^{s-1} \ .$$

We first consider the $K\alpha$ transitions of Al I to Al III, i.e., the $K\alpha$ lines of these ions with no holes in the L shell and with spectator electrons in the M shell. For these ions, the L shell is not an outer shell. It is expected that the transitions involving the excited configuration states with a $2p$ electron excited to the M shell have little contributions to the $K\alpha$ satellite line spectra. Hence, we only considered the $K\alpha$ transitions involving ground configuration states i.e., the transitions of type

$$1s^1 2s^2 2p^6 3l^N \rightarrow 1s^2 2s^2 2p^5 3l^N \ . \quad (15)$$

The calculated wavelengths and gf values of $K\alpha$ lines are given in Table IV. The corresponding stick spectrum is given in Fig. 3. It can be seen that the effect of removing electrons from the M shell on the $K\alpha$ lines is relatively

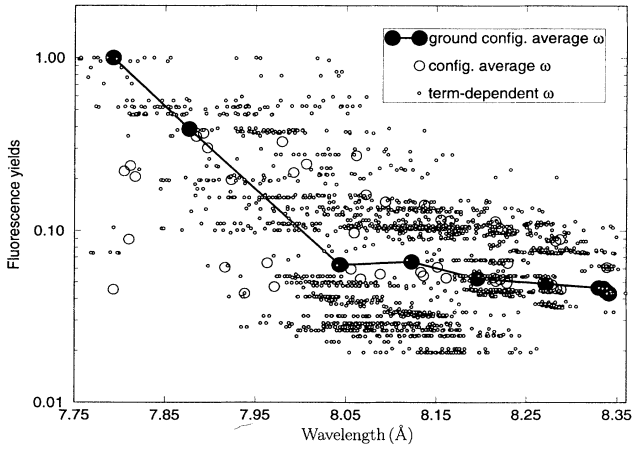

FIG. 2. Term-dependent, configuration-average, and ground-configuration-average fluorescence yields ω for Al I–Al XI.

TABLE IV. Calculated wavelength and gf values for the characteristic $K\alpha$ lines from Al I to Al IV.

Ion	Transition		Wavelength (Å)	gf
Al I	$1s^2 2s^2 2p^5 3s^2 3p^1$	$[^3D_1] \rightarrow 1s^1 2s^2 2p^6 3d^2 3p^1$	$[^3P_o]$	8.342	0.163
		$[^3P_1]$	$[^3P_2]$	8.345	0.104
		$[^3S_1]$	$[^3P_2]$	8.338	0.103
		$[^1P_1]$	$[^1P_1]$	8.342	0.113
		$[^3D_2]$	$[^3P_1]$	8.341	0.326
		$[^3P_2]$	$[^3P_1]$	8.343	0.167
		$[^1D_2]$	$[^1P_1]$	8.342	0.196
		$[^3P_2]$	$[^3P_2]$	8.343	0.246
		$[^1D_2]$	$[^3P_2]$	8.344	0.135
		$[^3D_3]$	$[^3P_2]$	8.341	0.578
Al II	$1s^2 2s^2 2p^5 3s^2$	$[^2P_{1/2}] \rightarrow 1s^1 2s^2 2p^6 3d^2$	$[^2S_{1/2}]$	8.341	0.164
		$[^2P_{3/2}]$	$[^2S_{1/2}]$	8.339	0.328
Al III	$1s^2 2s^2 2p^5 3s^1$	$[^3P_1] \rightarrow 1s^1 2s^2 2p^6 3s^1$	$[^3S_1]$	8.336	0.237
		$[^3P_2]$	$[^3S_1]$	8.336	0.431
		$[^1P_1]$	$[^1S_1]$	8.339	0.235
Al IV	$1s^2 2s^2 2p^5$	$[^2P_{1/2}] \rightarrow 1s^1 2s^2 2p^6$	$[^2S_{1/2}]$	8.331	0.173
		$[^2P_{3/2}]$	$[^2S_{1/2}]$	8.329	0.346

unimportant as the corresponding energy shifts of $K\alpha$ transitions from Al I to Al III are small. The $K\alpha$ lines cover a rather small range from 8.325 to 8.345 Å. By comparison with the PBFA-II experimental spectrum, these $K\alpha$ satellite lines are unresolvable and give a broad line which is asymmetric toward the short-wavelength side.

In the case of Al IV, there are no holes in the L shell in the ground configuration. Two $K\alpha$ lines are associated with the transition

$$1s^1 2s^2 2p^6 \rightarrow 1s^2 2s^2 2p^5 \ . \tag{16}$$

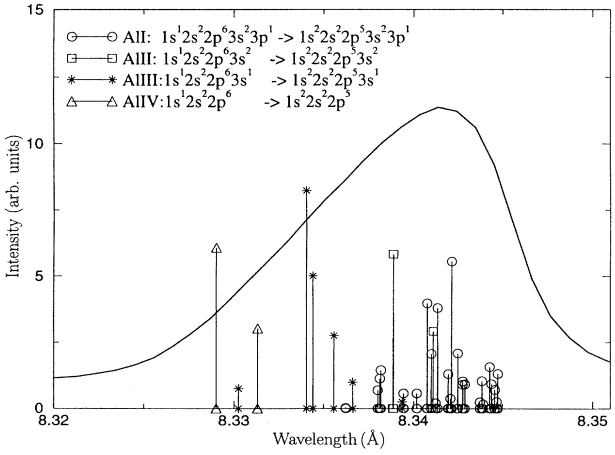

FIG. 3. $K\alpha$ lines for the transitions involving ground configuration states from Al I to Al IV. The broad line is the PBFA-II experimental spectrum.

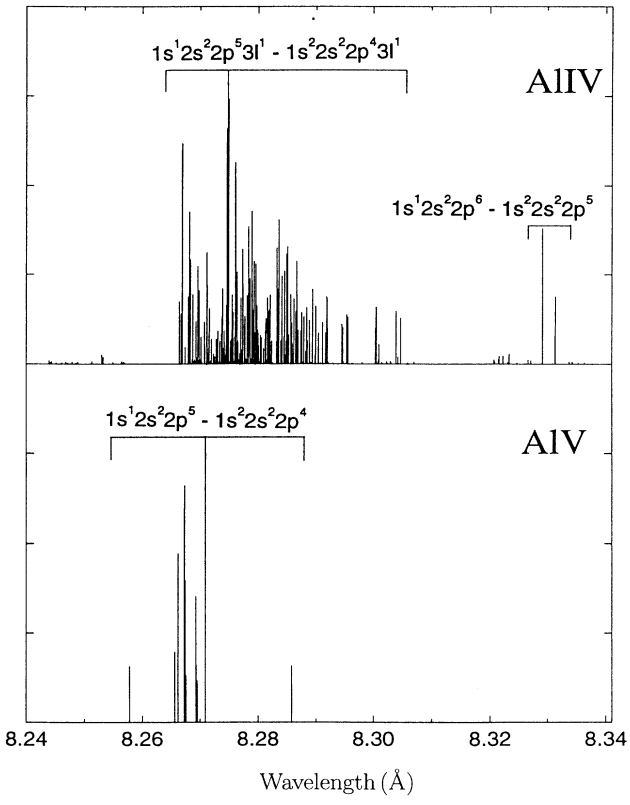

FIG. 4. Calculated wavelengths and relative intensities of $K\alpha$ satellite lines from Al IV and Al V. The lines are classified into groups.

Our calculation shows that these two lines overlap the wavelength range of Al I–Al III. On the other hand, since the L shell is an outer shell in the ground configuration, an L-shell hole can be easily produced by exciting a $2p$ electron to the M shell. In this case, we have $K\alpha$ lines related to the transition array

$$1s^1 2s^2 2p^5 3l^1 \rightarrow 1s^2 2s^2 2p^4 3l^1 , \quad (17)$$

where l represents s, p, or d subshell. There are about 200 lines associated with this transition array. The calculated line positions and the corresponding oscillator strengths for these $K\alpha$ lines will be published elsewhere [19]. In Fig. 4 we present the stick spectrum of $K\alpha$ lines for Al IV, along with the $K\alpha$ lines for the transitions

$$1s^1 2s^2 2p^5 \rightarrow 1s^2 2s^2 2p^4$$

and

$$1s^1 2s^1 2p^6 \rightarrow 1s^2 2s^1 2p^5$$

of Al IV. As shown, the structure of $K\alpha$ satellite lines for the transition array of

$$1s^1 2s^2 2p^5 3l^1 \rightarrow 1s^2 2s^2 2p^4 3l^1$$

is very complex. These satellite lines are blueshifted with respect to the $K\alpha$ lines of the ground configuration state of Al IV and strongly overlap the $K\alpha$ lines of Al IV. The blueshift effect is caused by the reduced screening of the nucleus, which results when a $2p$ electron is excited to the M shell or a higher shell. The overlapping effect results from the valence electron in M or a higher shell having little effect on the electronic wave functions in the inner regions of the ion, and therefore the effect of removing an electron from the M shell on $K\alpha$ transition energies is very small. Hence, there is no significant shift in transition energies from

$$1s^1 2s^2 2p^5 3l^1 \rightarrow 1s^2 2s^2 2p^4 3l^1$$

to

$$1s^1 2s^2 2p^5 \rightarrow 1s^2 2s^2 2p^4 .$$

This overlapping phenomenon of $K\alpha$ lines of Al IV and Al V may partially explain why the central peak of Al V lines in the PBFA-II experimental spectrum is asymmetric toward the long-wavelength side.

Our calculation shows that this overlapping phenomenon also appears for other ions in higher ionization stages. All the calculated results are summarized in Figs. 5–7. It can be seen from the Figures that the $K\alpha$ lines for a specific ionization stage can be classified into two groups. One is the characteristic group, which represents the characteristic $K\alpha$ line position of the ionization stage. The $K\alpha$ lines of this group are from the

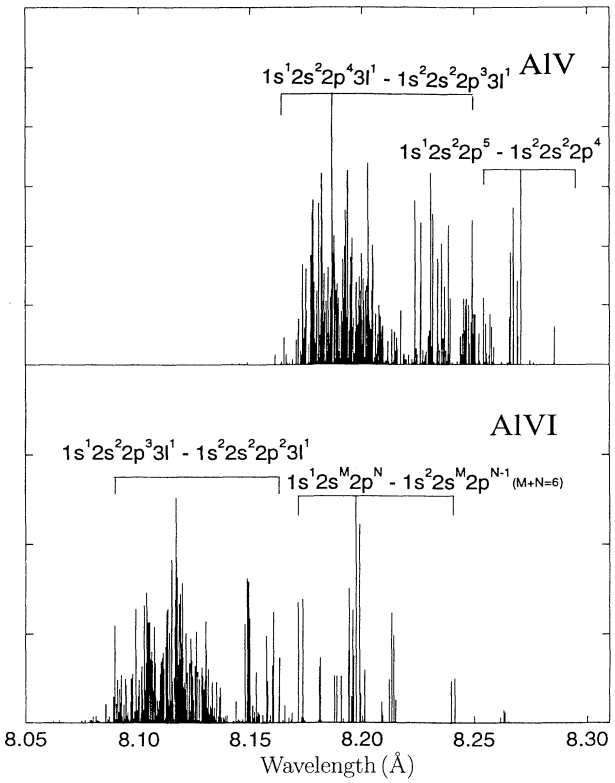

FIG. 5. Calculated wavelengths and relative intensities of $K\alpha$ satellite lines from Al V and Al VI. The lines are classified into groups.

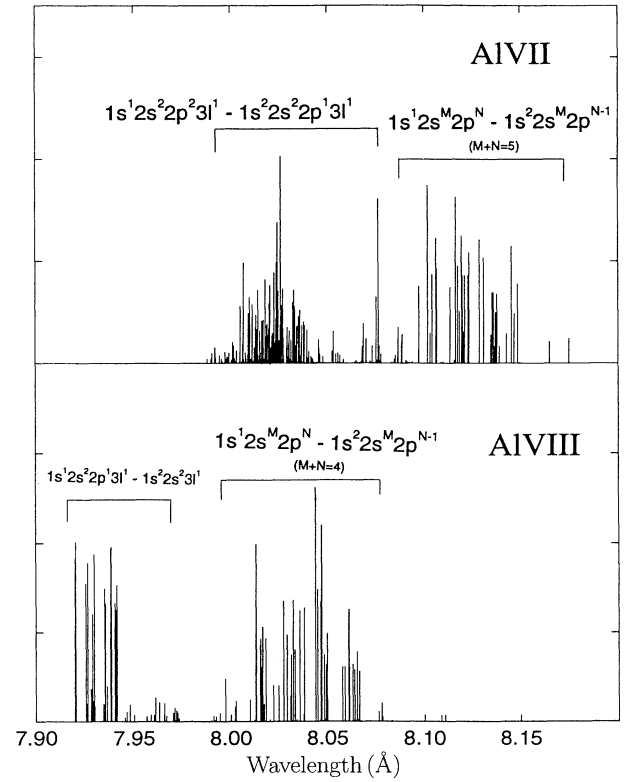

FIG. 6. Calculated wavelengths and relative intensities of $K\alpha$ satellite lines from AL VII and Al VIII. The lines are classified into groups.

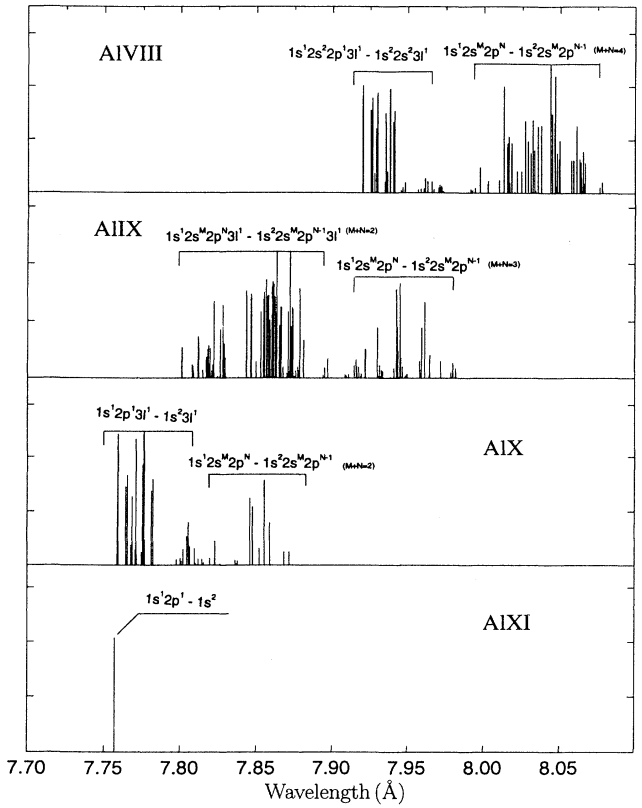

FIG. 7. Calculated wavelengths and relative intensities of $K\alpha$ satellite lines from Al VIII to Al XI. The lines are classified into groups as shown.

transitions involving the ground configuration states and the transitions involving excited configuration states with a $2s$ electron excited to a $2p$ subshell. Another is the overlapping group, which overlaps the characteristic $K\alpha$ lines of the next-higher ionization stage and affects the whole characteristic line shape. The $K\alpha$ lines of this group are from the transitions involving the excited configuration states with a $2p$ electron excited to the M shell or a higher shell. This overlapping phenomenon of $K\alpha$ lines of two consecutive ionization stages is important for the spectroscopy analysis of $K\alpha$ satellite spectra. It has been found [7,8] that the Stark broadening effect for the lines in the overlapping group is much stronger than that for the lines in the characteristic group. In a plasma of moderate to high density, the lines in overlapping groups show a much more pronounced dependence on electron density than those in characteristic groups. Thus, the $K\alpha$ lines in overlapping groups offer better opportunities for diagnosing plasma densities.

In Fig. 8 we present a stick spectrum which includes the $K\alpha$ lines of Al I to Al XI and compare with the PBFA-II experimental spectrum. It can be seen that very good agreement is attained. An important point to be noted in Fig. 8 is that each broad maximum in the experimental spectrum corresponds to a large number of overlapping $K\alpha$ satellite lines of two consecutive ionization stages. Studies [7,8] have shown that overlapping satellite

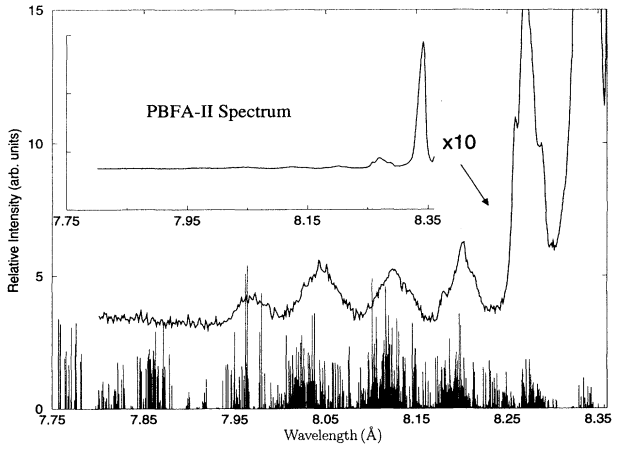

FIG. 8. A theoretically calculated $K\alpha$ satellite spectrum of aluminum. Upper portion: PBFA-II experimental $K\alpha$ spectrum.

lines play an important role for the broad feature of the $K\alpha$ satellite lines in the experimental spectrum; there could not be any reasonable fit to the experimental data without taking account of the contributions of the overlapping satellite lines. Other effects, such as the opacity effect and the time-integration effect, can also contribute to the broad line shape. Our calculation also shows that the peak with the shortest wavelength in the experimental spectrum is actually attributed to the $K\alpha$ transition of ground configuration states of Al IX, excited states of Al VIII, and the $K\beta$ transition of Al I.

IV. CONCLUSIONS

In order to analyze the experimental aluminum $K\alpha$ spectrum of a PBFA-II experiment, it is necessary to understand the detailed structure of $K\alpha$ satellite lines of aluminum ions. We have performed relativistic configuration-interaction (CI+BP) calculations to determine the transition energies, oscillator strengths, and fluorescence yields for the $K\alpha$ transitions of aluminum ions up to He-like Al. It has been shown that both relativistic and correlation effects significantly impact the calculated $K\alpha$ transition energies. Our calculated wavelengths for the most prominent $K\alpha$ transitions agree well with the strongest features observed in the PBFA-II experimental spectrum. We have calculated the properties for $K\alpha$ lines of both ground configurations and excited-state configurations. It has been shown that for ions with the L shell being an outer shell (Al IV to Al XI), the corresponding $K\alpha$ satellite lines can be classified into characteristic and overlapping groups. The characteristic group, which is associated with the lines of transitions involving ground configuration states, can be used for characterizing the ionization stage. The overlapping group, which is associated with the $K\alpha$ lines of transitions involving excited configuration states with M-shell spectator electrons, has substantial contributions to the observed $K\alpha$ spectrum from optically thick targets, and can have important effects on the line shape of the $K\alpha$ sa-

tellite spectrum [8].

Our calculated results have been used to simulate the $K\alpha$ experimental spectrum of a PBFA-II experiment using a collisional-radiative-equilibrium (CRE) model in conjunction with hydrodynamics simulations [8]. Good agreement with the experimental spectrum is attained. With the use of our theoretical wavelengths, oscillator strengths, and fluorescence yields, we can identify lines in the $K\alpha$ spectra and determine relative intensities of different prominent $K\alpha$ lines. This provides us the possibility of using $K\alpha$ line ratios to diagnose temperatures and densities in light-ion beam-heated plasmas. Further studies along these lines are currently under way.

ACKNOWLEDGMENTS

This work has been supported in part by Sandia National Laboratories and by Kernforschungszentrum Karlsruhe (FRG) through Fusion Power Associates. Computing support was provided in part by the National Science Foundation through the San Diego Supercomputer Center.

[1] J. Abdallah, Jr., R. E. H. Clark, and J. M. Peek, Phys. Rev. A **44**, 4072 (1991).
[2] T. S. Perry, S. J. Davidson, F. J. D. Serduke, D. R. Bach, C. C. Smith, J. M. Foster, R. J. Doyas, R. A. Ward, C. A. Iglesias, F. J. Rogers, J. Abdallah, Jr., R. E. Stewart, J. D. Kilkenny, and R. W. Lee, Phys. Rev. Lett. **67**, 3784 (1991).
[3] C. Chenais-Popovics, C. Fievet, J. P. Geindre, and J. C. Gauthier, E. Luc-Koenig, J. F. Wyart, H. Pepin, and M. Chaker, Phys. Rev. A **40**, 3194 (1989).
[4] D. M. O'Neil, C. L. S. Lewis, D. Neely, and S. J. Davidson, Phys. Rev. A **44**, 2641 (1991).
[5] E. Nardi and Z. Zinamon, J. Appl. Phys. **52**, 7075 (1981).
[6] J. Bailey, A. L. Carlson, G. Chandler, M. S. Derzon, R. J. Dukart, B. A. Hammel, D. J. Johnson, T. R. Lockner, J. Maenchen, E. J. McGuire, T. A. Mehlhorn, W. E. Nelson, L. E Ruggles, W. A. Stygar, and D. F. Wenger, Lasers Part. Beams **8**, 555 (1990).
[7] R. Mancini (private communication).
[8] J. J. MacFarlane, P. Wang, J. Bailey, T. A. Mehlhorn, R. J. Dukart, and R. Mancini, Phys. Rev. E **47**, 2748 (1993).
[9] W. J. Kuhn and B. L. Scott, Phys. Rev. A **34**, 1125 (1986).
[10] B. L. Scott, Phys. Rev. A **34**, 4438 (1986).
[11] C. F. Fischer, Comput. Phys. Commun. **14**, 145 (1978).
[12] S. Fraga, M. Klobukowski, J. Muszynsha, K. M. S. Saxena, J. A. Sordo, and J. D. Climenhaga, Comput. Phys. Commun. **47**, 159 (1987).
[13] J. F. Perkins, J. Chem. Phys. **45**, 2156 (1965).
[14] R. Glass and A. Hibbert, Comput. Phys. Commun. **16**, 19 (1978).
[15] S. Fraga, M. Klobukowski, J. Muszynsha, K. M. S. Saxena, and J. A. Sordo, Phys. Rev. **34**, 23 (1986).
[16] W. N. Asaad and E. H. S. Burhop, Proc. R. Soc. London **71**, 369 (1958).
[17] M. Klapisch, J. L. Schwob, B. S. Fraenkel, and J. Oreg, J. Opt. Soc. Am. **67**, 148 (1977).
[18] F. Combet Farnoux, J. Phys. (Paris) Colloq. Suppl. **12**, C9-199 (1987).
[19] P. Wang, J. J. MacFarlane, and G. A. Moses (unpublished).